

1 Phosphorylation induces structural changes in the Autographa californica nucleopolyhedrovirus  
2 P10 protein

3

4

5 Farheen Raza,<sup>a\*</sup> Joanna F. McGouran,<sup>b\*\*</sup> Benedikt M. Kessler,<sup>b</sup> Robert D. Possee,<sup>a</sup> Linda A.  
6 King<sup>a#</sup>

7

8 Department of Biological & Medical Sciences, Oxford Brookes University, Oxford, UK<sup>a</sup>; Target  
9 Discovery Institute, Nuffield Department of Medicine, University of Oxford, Roosevelt Drive,  
10 Oxford OX3 7FZ, UK<sup>b</sup>

11

12 Running Head: Phosphorylation of AcMNPV P10

13

14 #Address correspondence to Linda A King, [laking@brookes.ac.uk](mailto:laking@brookes.ac.uk).

15 \*Present address: Medical Research Council Toxicology Unit, Hodgkin Building, Lancaster  
16 Road, Leicester LE1 9HN, UK.

17 \*\*Present address: School of Chemistry, Trinity College Dublin, University of Dublin, College  
18 Green, Dublin 2, Ireland

19

20 Word count for abstract: 195

21 Word count for rest of text: 5371

22

23

24

25 **Structured Abstract**

26 **Abstract**

27 Baculoviruses encode a variety of auxiliary proteins that are not essential for viral replication but  
28 provide them with a selective advantage in nature. P10 is a 10 kDa auxiliary protein produced in  
29 the very-late phase of gene transcription by *Autographa californica* multiple  
30 nucleopolyhedrovirus (AcMNPV). The P10 protein forms cytoskeletal-like structures in the host  
31 cell that associate with microtubules varying from filamentous forms in the cytoplasm to  
32 aggregated peri-nuclear tubules that form a cage-like structure around the nucleus. These P10  
33 structures may have a role in the release of occlusion bodies (OBs) and thus mediate horizontal  
34 transmission of the virus between insect hosts. Here it is demonstrated, using mass spectrometric  
35 analysis, that the C-terminus of P10 is phosphorylated during virus infection of cells in culture.  
36 Analysis of the P10 mutants encoded by recombinant baculoviruses in which putative  
37 phosphorylation residues were mutated to alanine showed that serine 93 is a site of  
38 phosphorylation. Confocal microscopy examination of the serine 93 mutant structures revealed  
39 an aberrant formation of the peri-nuclear tubules. Thus, phosphorylation of serine 93 may induce  
40 aggregation of filaments to form tubules. Together, these data suggest that the phosphorylation of  
41 serine 93 affects P10 structural conformation.

42

43 **Importance**

44 The baculovirus P10 protein has been researched intensively since it was first observed in 1969,  
45 but its role during the viral infection remains unclear. It is conserved in the alphabaculoviruses  
46 and expressed at high levels during virus infection. Producing large amounts of a protein is  
47 wasteful for the virus unless it is advantageous for survival of its progeny and therefore P10  
48 presents an enigma. As P10 polymerises to form organised cytoskeletal structures that co-localise

49 with the host cell microtubules, the structural relationship of the protein with the host cell may  
50 present a key to help understand the function and importance of this protein. This study  
51 addresses the importance of the structural changes in P10 during infection and how they may be  
52 governed by phosphorylation. The P10 structures affected by phosphorylation are closely  
53 associated with the viral progeny and thus, potentially, be responsible for its dissemination and  
54 survival.

55

## 56 **Introduction**

57 *Autographa californica* multiple nucleopolyhedrovirus (AcMNPV) is a model alphabaculovirus  
58 and belongs to the family of *Baculoviridae*. This family of viruses is characterised by a circular  
59 double-stranded DNA genome enclosed in a rod-shaped capsid and further enveloped by a  
60 membrane (1). The replication cycle of baculoviruses produces two forms of progeny virus: the  
61 budded virus (BV) and the occlusion-derived virus (ODV) (2, 3). The ODV is protected within a  
62 protein-rich matrix forming an occlusion body (OB) that is either polyhedral  
63 (nucleopolyhedroviruses) or granular (granuloviruses) in shape (4). Transcription of some  
64 baculovirus genes, notably *polyhedrin (ac8)* and *p10 (ac137)*, occurs in a very-late phase that  
65 initiates approximately six hours after the onset of late gene transcription (5). While the role of  
66 polyhedrin as an OB matrix protein is well-established, the P10 protein remains poorly  
67 understood. P10 is a 10 kDa protein that forms cytoskeletal-like fibrillar structures in virus-  
68 infected cells and together with polyhedrin accounts for the majority of the virus-encoded  
69 protein present in the host cell during the very-late phase (6).

70

71 Homologues of *p10* were reported in 27 alpha- and 2 beta-baculovirus genomes (7); however, we  
72 found a further 25 homologues (19 alpha- and 6 beta-baculovirus) in the NCBI protein database  
73 (Table 1).

74

75 Baculovirus replication can occur in the absence of P10 (8), but studies have indicated that P10  
76 may have a number of roles in the very-late stages of the replication cycle (8–10). P10 has been  
77 implicated in nuclear lysis as *Spodoptera frugiperda* cells infected with a recombinant AcMNPV  
78 lacking *p10* failed to release OBs, even at two weeks post-infection (9). In contrast, cells infected  
79 with the wild-type AcMNPV released large numbers of OBs at two days post-infection.

80

81 Early transmission electron microscopy (TEM) studies of the P10 protein structure reported a  
82 close association between the polyhedron envelope (PE) and P10 (8–10). Virus infection of  
83 *Trichoplusia ni* cells with an AcMNPV *p10* deletion mutant resulted in poor attachment of the  
84 PE to the surface of polyhedra (9). Studies utilising scanning EM demonstrated that the  
85 polyhedra from *Orgyia pseudotsugata* larvae infected with a *p10*-deficient recombinant O.  
86 pseudotsugata (Op) MNPV had pitted surfaces, from dislodging of virions, whereas the wild-  
87 type polyhedra had smooth surfaces (10).

88

89 Although P10 fibrillar structures have been described through TEM analyses dating from 1969  
90 (11), immunofluorescence microscopy images first appeared in a study by Quant-Russell *et al.*  
91 (12) . In OpMNPV-infected *Lymantria dispar* cells, P10 structures were first detected at 14 hpi  
92 as ‘fine threads’ in the cytoplasm and by 16 hpi these structures had ‘condensed into thicker rod-  
93 like’ structures that form an ‘interconnected network’ at later stages (12). Subsequent studies by  
94 Patmanidi *et al.* (13) and Carpentier *et al.* (14) employed confocal immunofluorescence

95 microscopy to analyse P10 structures in AcMNPV-infected *S. frugiperda* and *T. ni* cells,  
96 respectively. The P10 filamentous structures were evident at 18 hpi in AcMNPV-infected *T.ni*  
97 cells (TN368 cell line), and these had formed a network in the cytoplasm by 30 hpi followed by  
98 distinctive peri-nuclear aggregates or tubules by 36 hpi (14).

99

100 A study by Cheley *et al.* (15) revealed that *S. frugiperda* cells infected with a recombinant  
101 AcMNPV encoding the catalytic subunit of *Aplysia* protein kinase A (PKA) developed cellular  
102 projections. Analysis of these cells using TEM showed that these projections were a result of  
103 extended microtubules (MTs). Moreover, [<sup>32</sup>P] orthophosphate labelling of taxol-stabilised MTs  
104 from cells infected with the PKA recombinant baculovirus showed high levels of phosphorylated  
105 P10. However, no phosphorylated P10 was observed in MTs prepared from cells infected with  
106 the wild-type virus. These data allowed the authors to conclude that the cellular projections were  
107 a result of MT elongation induced by phosphorylated P10. Additionally, it was shown that P10  
108 was phosphorylated by *Aplysia* PKA at the C-terminus. Further analysis of the virus-infected  
109 cells revealed that phosphorylated P10 associated with MTs, but it could not bundle them.  
110 Interaction of P10 with MTs during the wild-type virus infection was later confirmed in *S.*  
111 *frugiperda* and *T. ni* cells (13, 14). These studies demonstrated that the initial P10 filamentous  
112 structures in the cytoplasm co-align with MTs. Furthermore, formation of the P10 filamentous  
113 structures was inhibited upon treatment with colchicine, which inhibits microtubule  
114 polymerization (14). Together, these data suggest that P10's interaction with MTs is important  
115 to its formation and stabilisation.

116

117 The work by Cheley *et al.*, (15) showed that phosphorylation of P10 by *Aplysia* PKA affected the  
118 P10 structure. It is not known whether this phenomenon occurs in a wild-type AcMNPV

119 infection and in a natural AcMNPV host. In this study we provide evidence for P10  
120 phosphorylation in AcMNPV infection of *T. ni* cells via mass spectrometric analysis and also  
121 identify the phospho-acceptor site within P10. The structural consequences of P10  
122 phosphorylation were investigated through alanine mutagenesis and confocal microscopy.

123

## 124 **Material and Methods**

125

### 126 **Cells and viruses**

127

128 This study utilised cell lines derived from the ovary of *T. ni* (High Five™, TN368). TN368 (19)  
129 cells were grown in TC-100 Insect Medium (Gibco®) with 10% (v/v) fetal bovine serum  
130 (Sigma-Aldrich) as adherent culture. High Five™ (18) cells were grown in EX-CELL® 405  
131 (Sigma-Aldrich) as suspension culture. Sf9 (16) and Sf21 (17) cells, derived from the ovary of *S.*  
132 *frugiperda*, were used in the process of recombinant baculovirus generation and plaque assay.  
133 Sf9 cells were grown in InsectExpress Sf9-S2 (PAA), and Sf21 cells in TC-100 Insect Medium  
134 (Gibco®) with 10% (v/v) fetal bovine serum (Sigma-Aldrich). Both Sf21 and Sf9 were  
135 maintained as suspension cultures. The wild-type virus used in this work was AcMNPV C6 (20).

136

### 137 **Site-directed mutagenesis of *p10* and generation of recombinant viruses**

138 In summary, site directed mutagenesis was performed using the QuikChange kit (Stratagene)  
139 according to the method described by Vandeyar *et al.* (21). In essence, DNA was synthesised in a  
140 PCR using a high fidelity *Pfu* DNA polymerase (Agilent Technologies) and custom primers.  
141 This was treated with *DpnI* endonuclease to digest the parental DNA template. The *DpnI*-treated

142 DNA was used to transform competent bacterial cells. All mutations were confirmed by DNA  
143 sequencing.

144  
145 The plasmid pCRII-TOPO-P10<sup>wt</sup> was constructed by sub-cloning of the *p10* gene (amplified  
146 from the AcMNPV strain C6) into pCRII-TOPO (Invitrogen) using the *Xba*I and *Eco*RI  
147 restriction sites. The *p10* codons for serine 92 and 93 were then each mutated to specify alanine.  
148 In the first step, serine 92 was mutated to alanine in a PCR reaction using P10\_S92AF and  
149 P10\_S92AR primers (Table 2). In a second PCR reaction serine 93 was mutated to alanine using  
150 P10\_S93AF and P10\_S93AR primers. The resulting plasmid was named pCRII-TOPO-  
151 P10<sup>S9293A</sup>.

152  
153 The modified *p10* fragment was amplified from the plasmid pCRII-TOPO-P10<sup>S9293A</sup> using  
154 P10\_S9293A\_pBP8F and P10\_S9293A\_pBP8R primers in a PCR. The product was digested  
155 with *Xba*I and *Xma*I and then sub-cloned into pBacPAK8, downstream of the polyhedrin  
156 promoter, to generate pBacPAK8-P10<sup>S9293A</sup>.

157  
158 The plasmid pBacPAK8-P10<sup>S9293A</sup> was used to generate single P10 mutants in which either  
159 serine 92 or 93 codons were mutated to specify alanine instead. Single mutations were created  
160 through site-specific mutagenesis using P10\_S92A\_pBP8F and P10\_S92A\_pBP8R primers to  
161 derive pBacPAK8-P10<sup>S92A</sup>, and P10\_S93A\_pBP8F and P10\_S93A\_pBP8R to derive  
162 pBacPAK8-P10<sup>S93A</sup>.

163

164 To generate a control, the *p10* gene was amplified from pCRIITOPPO-P10<sup>wt</sup> using P10\_wtF and  
165 P10\_wtR primers. The PCR product was digested with *Xba*I and *Xma*I and then sub-cloned into  
166 pBacPAK8 downstream of the polyhedrin gene promoter to derive pBacPAK8-P10<sup>wt</sup>.

167  
168 The plasmids pBacPAK8-P10<sup>S9293</sup>, pBacPAK8-P10<sup>S92A</sup>, pBacPAK8-P10<sup>S93A</sup> and pBacPAK8-  
169 P10<sup>wt</sup> were used in a co-transfection with *flash*BACULTRA genomic DNA (Oxford Expression  
170 Technologies Ltd) to generate recombinant viruses. These viruses were designated AcP10<sup>S9293A</sup>,  
171 AcP10<sup>S92A</sup>, AcP10<sup>S93A</sup> and AcP10<sup>wt</sup>, respectively.

172  
173 To construct polyhedrin positive viruses, *p10* was amplified from the plasmid pBacPAK8-P10<sup>wt</sup>  
174 using P10\_wt\_pW2BF and P10\_wt\_pW2BR primers in a PCR. The DNA product was digested  
175 with *Pst*I (this restriction site was introduced into the plasmid pAcUW2B through site-specific  
176 mutagenesis) and inserted into pAcUW2B, downstream of the *p10* promoter to derive  
177 pAcUW2B-P10<sup>wt</sup>. This plasmid was then used to generate the *p10* mutants. The P10 residue,  
178 serine 93, was mutated to alanine through site-specific mutagenesis using P10\_S93A\_pW2BF  
179 and P10\_S93A\_pW2BR primers to derive pAcUW2B-P10<sup>S93A</sup>.

180  
181 To derive a pAcUW2B transfer vector encoding polyhistidine-tagged P10 (wild-type and serine  
182 93 mutant), plasmids pAcUW2B-P10<sup>wt</sup> and pAcUW2B-P10<sup>S93A</sup> were used. The wild-type *p10*  
183 gene was PCR amplified from the plasmid pAcUW2B-P10<sup>wt</sup> using HISP10\_wt\_pW2BF and  
184 HISP10\_wt\_pW2BR primers introducing a 6x histidine tag and a TEV cleavage site at the N-  
185 terminus. The PCR fragment and pAcUW2B were digested with *Pst*I and *Spe*I and ligated  
186 together to produce pAcUW2B-His-P10<sup>wt</sup>. The serine 93 mutant *p10* was PCR amplified from  
187 the plasmid pAcUW2B-P10<sup>S93A</sup> using HISP10\_S93A\_pW2BF and HISP10\_S93A\_pW2BR



188 primers introducing a 6x histidine tag and a TEV cleavage site at the N-terminus. The PCR  
189 fragment and pAcUW2B were digested with *Pst*I and *Spe*I; the fragment was then ligated into  
190 pAcUW2B, downstream of the *p10* promoter to derive pAcUW2B-His-P10<sup>S93A</sup>. Recombinant  
191 viruses (AcUW2B-His-P10<sup>wt</sup> and AcUW2B-His-P10<sup>S93A</sup>) were generated as described above.

192

### 193 **Generation of recombinant viruses**

194 Cell cultures dishes (35 mm) were seeded with Sf9 cells at a density of 0.5x10<sup>6</sup> ml<sup>-1</sup>. Co-  
195 transfection mixtures were prepared using 1 ml of appropriate cell culture medium, 5 µl of  
196 Lipofectin® reagent (Invitrogen), 100 ng of *flashBACULTRA*<sup>TM</sup> (Oxford Expression  
197 Technologies Ltd) and 500 ng of transfer vector according to the method described by King and  
198 Possee (22). The medium containing the recombinant virus was collected on the fifth day.  
199 Viruses were amplified in Sf9 cell cultures and titres were determined by plaque assay in plaque-  
200 forming units (pfu) ml<sup>-1</sup> using Sf21 cells.

201

### 202 **Immunofluorescence**

203 For confocal immunofluorescence microscopy, TN368 cells were employed. These were seeded  
204 on glass coverslips (22 mm diameter) in 35 mm cell culture dishes at a density of 1x10<sup>5</sup> ml<sup>-1</sup> and  
205 were allowed to settle overnight at 28°C. To infect cells, the medium was removed from the  
206 dishes and 100 µl of appropriate dilution of the virus inoculum was added drop-wise onto the  
207 cells. For mock infection, 100 µl of cell culture medium was used. Cells were infected with each  
208 type of virus in triplicate. Cells were incubated at room temperature for 1 hour to allow virus  
209 adsorption. The inoculum was then removed and 2 ml of fresh media were added to the cells  
210 (this time point was defined as 0 hpi). Cells were incubated at 28°C until the desired time-point,  
211 medium was removed from the dishes and cells were washed twice with 1 ml of phosphate

212 buffered saline (PBS). For chemical fixation, cells were treated with 1 ml of 4% (v/v)  
213 paraformaldehyde for 1 hour, washed once with 1 ml of PBS and stored at 4°C until required for  
214 immunostaining.

215  
216 Tubulin was stained using a mouse monoclonal anti- $\alpha$ -Tubulin antibody (Sigma-Aldrich) and an  
217 anti-mouse Alexa Fluor 568 (Invitrogen). P10 was stained using a guinea pig polyclonal  
218 antibody (13) and an anti-guinea pig Alexa Fluor 488 (Invitrogen). For immunofluorescence  
219 staining, fixed cells were treated with a permeabilisation buffer (1% (w/v) bovine serum albumin  
220 and 0.1% (v/v) Triton X-100 in PBS) for 10 minutes. Cells were washed with 1 ml of PBS  
221 followed by 1 ml of 1% (w/v) BSA in PBS (PBS-BSA). Cells were probed with primary  
222 antibody, diluted in PBS-BSA, for 50 minutes. Unbound antibody was removed by washing cells  
223 with PBS-BSA three times. Cells were probed with secondary antibody diluted in PBS-BSA for  
224 50 minutes and then washed three times with PBS. Following immunofluorescence staining,  
225 coverslips were mounted on glass slides using the Vectashield mounting media (Vector  
226 Laboratories). Coverslips were sealed using a clear nail varnish and slides were stored at 4°C  
227 protected from light.

228

### 229 **Confocal microscopy**

230 Confocal laser scanning microscopy of immunostained cells was performed using the Zeiss LSM  
231 510 META system with an Axio Imager-Z1 upright microscope. Images were acquired using the  
232 oil immersion objectives EC Plan-Neofluar 40x (1.3 numerical aperture) or Plan-Apochromat  
233 63x (1.4 numerical aperture). A multi-track setup was employed to prevent signal cross-over.  
234 Fluorescence from Alexa Fluor 488 and Alexa Fluor 568 was recorded through the laser lines  
235 488- and 543 nm, respectively. Projection 3D images were generated using the Zeiss LSM Image

236 Browser (v4.2). Images shown were selected to be representative from a large number of  
237 individual cells examined (n>100).

238

### 239 **Mass spectrometry**

240 Coomassie stained protein gel bands of P10 were excised and cut into small pieces (1–2mm<sup>3</sup>)  
241 and transferred to a 1.5 ml tube. Gel pieces were shaken vigorously for 18 hours in destaining  
242 solution (1ml, 50% (v/v) methanol, 5% (v/v) acetic acid). Further destaining was carried out for  
243 2-3 hours with fresh destaining solution. The destaining solution was removed and gel pieces  
244 were dehydrated in 200 µl of acetonitrile for 5 minutes. Acetonitrile was removed and the  
245 dehydration step repeated. Reduction was carried out with 30 µl of 10 mM dithiothreitol buffer  
246 for 30 minutes. Reduction buffer was removed and replaced with alkylation buffer; alkylation  
247 was carried out with 30 µl of 50 mM iodoacetamide buffer for 30 minutes. Alkylation buffer was  
248 removed and gel pieces were dehydrated in 200 µl acetonitrile for 5 minutes. Acetonitrile was  
249 removed and gel pieces were rehydrated in 200 µl of 100 mM ammonium bicarbonate solution  
250 for 10 minutes. The dehydration step was repeated with 200 µl acetonitrile for 5 minutes and the  
251 solution was removed.

252

253 Digestion was carried out using a *Staphylococcus aureus* protease V8, endoproteinase GluC  
254 (NEB) which was prepared by adding 1 ml of ice-cold 50 mM ammonium bicarbonate to 20 µg  
255 of GluC (final concentration 20 ng/µl). Gel pieces were rehydrated with 30 µl of GluC solution  
256 on ice for 10 minutes and then briefly centrifuged to allow removal of excess enzyme solution.  
257 After adding 5 µl of 50 mM ammonium bicarbonate buffer solution to the gel pieces, digestion  
258 was performed at 37 °C for 18 hours.

259

260 Peptides were extracted from the gel pieces during each of the three successive 10 minute  
261 incubations of: (1) 50 µl of 50 mM ammonium bicarbonate buffer, (2) 50 µl of extraction buffer  
262 1 (50% (v/v) acetonitrile, 5% (v/v) formic acid) and (3) 50 µl of extraction buffer 2 (85% (v/v)  
263 acetonitrile, 5% (v/v) formic acid). The peptide solution was dried completely in a vacuum  
264 centrifuge and resuspended in 20 µl of a buffer solution (2% (v/v) acetonitrile, 0.1% (v/v) formic  
265 acid).

266

267 For matrix assisted laser desorption/ionization time-of-flight (MALDI-TOF) mass spectrometry  
268 analysis, 1 µl of peptide solution was mixed with 1 µl of matrix ( $\alpha$ -cyano-4-hydroxycinnamic  
269 acid) and spotted on a MALDI target. Samples were measured by MALDI-TOF (Ultraflex™,  
270 Bruker Daltonics) in linear mode. The MALDI-TOF spectra were analysed using the  
271 flexAnalysis software (Bruker Daltonics).

272

### 273 **Protein purification**

274 A shaking suspension culture of *T. ni* High Five™ cells was set up at a density of  $0.5 \times 10^6$  cells  
275 ml<sup>-1</sup> in a total volume of 500 ml. Cells were infected with the virus expressing the His-tagged  
276 protein at an MOI of 5 and incubated at 28°C. At the required time-point, cells were harvested by  
277 centrifugation at 10,000 xg for 15 minutes. The supernatant was removed and cells were washed  
278 with 50 ml of ice-cold PBS. Cells were lysed with a CytoBuster™ Protein Extraction Reagent  
279 (Novagen) and spun at 14,000 xg for 30 minutes to remove all insoluble material. After  
280 centrifugation, supernatant was filtered through a 0.45 µm membrane to prevent clogging of  
281 purification resin in subsequent steps. His-tagged protein purification was carried out using the  
282 His-Bind® purification kit (Novagen) according to the manufacturer's instructions. In brief, an  
283 iminodiacetic acid (IDA) agarose resin was used in a spin column to purify His-tagged proteins.

284 The IDA agarose resin was activated with a charge buffer (50 mM NiSO<sub>4</sub>) and equilibrated with  
285 a binding buffer (0.5 M NaCl, 20 mM Tris-HCl, 5 mM imidazole, pH 7.9). Prepared soluble  
286 lysates were passed through the spin column. The resin was treated with the binding buffer and  
287 then wash buffer (0.5 M NaCl, 60 mM imidazole, 20 mM Tris-HCl, pH 7.9) to remove any non-  
288 specific binding of proteins with the resin. Elution was performed with the buffer containing 400  
289 mM imidazole, 0.5 M NaCl, 20 mM Tris-HCl at pH 7.9. Purified protein was assessed for purity  
290 through Coomassie staining.

291

## 292 **Circular Dichroism**

293 Circular dichroism (CD) spectra were recorded on a Jasco J-720 spectropolarimeter (Jasco  
294 GmbH) using a 0.05 cm path length quartz cell. Spectra of a 100 µg ml<sup>-1</sup> protein solution in 10  
295 mM phosphate buffer were averaged from 4 to 16 scans (260–190 nm) and corrected using a  
296 buffer blank. The CD spectra were analysed on the CD analyser system (V2.02) software using  
297 the LINCOMB method (23).

298

## 299 **Results**

300

### 301 **1. Temporal analysis of P10 structures by confocal microscopy**

302 Wild-type AcMNPV P10 structures in virus-infected cells were analysed by laser scanning  
303 confocal microscopy to visualise the major changes that occur from their peak expression time at  
304 48 hpi (24) until they are semi-disintegrated, typically at 96 hpi (Figure 1), extending previous  
305 studies which examined P10 structures until 72 hpi (14). TN368 cells were infected in triplicate  
306 culture dishes with AcMNPV at a multiplicity of infection (MOI) of 10 pfu cell<sup>-1</sup>, fixed at 48-,  
307 72- and 96 hpi, and then immunostained to detect P10 and host MTs.

308

309 At 48 hpi (Fig. 1, left hand panels), P10 formed filamentous structures in the cytoplasm and  
310 around the nucleus of the host cell. Aggregated filaments were also observed surrounding the  
311 nucleus. The orientation of P10 filaments in the cytoplasm was similar to that of the host MTs  
312 and thus both were co-aligned, most prominently in regions of stable MTs. At 72 hpi (Fig. 1,  
313 centre panels), the P10 cytoplasmic filaments showed further bundling and were still co-aligned  
314 with MTs. At this time-point, thicker tubule-like structures, possibly resulting from aggregation  
315 of finer P10 filaments, were also observed surrounding the OB-filled nucleus. At 96 hpi (Fig. 1,  
316 right hand panels), the P10 peri-nuclear tubular structures had fully matured, and the cytoplasmic  
317 filaments were mostly detached and/or disintegrated. Some detached filaments had a loop-like  
318 terminal structure. Additionally, a layer of P10 was also observed enveloping the OBs inside the  
319 host nucleus at 72- and 96 hpi.

320

## 321 **2. Phosphorylation of P10 in wild-type AcMNPV infection**

322 This study utilised MALDI-TOF mass spectrometry to analyse changes in the mass of the P10 C-  
323 terminus that Cheley *et al.* (15) had reported to be the domain phosphorylated by *Aplysia* PKA.  
324 Analysis of the amino acid sequence of P10 showed that the C-terminus contained three potential  
325 phosphorylation sites at serine 70, 92 and 93. For MALDI-TOF analysis, *T. ni* cells were infected  
326 with wild-type AcMNPV at an MOI of 10 and harvested at 72 hpi. This time-point was selected  
327 as it showed both forms of P10 structures (Figure 1). Lysates were separated using SDS-PAGE  
328 and stained with Coomassie solution. Digestion of P10 protein was carried out using the  
329 endoproteinase GluC (*Staphylococcus aureus* protease V8) to cleave peptide bonds C-terminal to  
330 glutamic acid residues. The MALDI-TOF spectrum was analysed for peaks corresponding to the  
331 C-terminal peptide containing serine 92 and 93 residues.

332

333 Figure 2 shows a MALDI-TOF spectrum containing the m/z peaks (labelled) corresponding to  
334 the C-terminal peptide  $^{82}\text{LDSDARRGKRSSK}^{94}$ , a product of the endoproteinase GluC digestion  
335 of P10. The MALDI-TOF spectrum shows a peak ( $[\text{M}+\text{H}]^+$  1475.81) corresponding to the  
336 peptide  $^{82}\text{LDSDARRGKRSSK}^{94}$  (calculated mass 1475.80). Phosphorylation of the P10 C-  
337 terminus was confirmed by the presence of the peak  $[\text{M}+\text{H}]^+$  1555.75 corresponding  
338 to  $^{82}\text{LDSDARRGKRSSK}^{94} + 1\text{P} (\text{PO}_3^{2-})$  (calculated mass 1555.77). This finding suggests that  
339 either serine 92 or serine 93 in the peptide  $^{82}\text{LDSDARRGKRSSK}^{94}$  is a phospho-acceptor site of  
340 the P10 protein. Another peptide,  $^{55}\text{IQSILTGDIVPDLPSLKPCLKSQAPE}^{81}$ , was also  
341 examined using MALDI-TOF but did not reveal a form consistent with phosphorylation of serine  
342 70 (data not shown).

343

### 344 **3. Temporal analysis of P10 mutant structures by confocal microscopy**

345 Recombinant viruses were generated containing serine-alanine mutations at positions 92 and 93  
346 or at both residues within P10 (Figure 3). These viruses,  $\text{AcP10}^{\text{S9293A}}$ ,  $\text{AcP10}^{\text{S92A}}$ ,  $\text{AcP10}^{\text{S93A}}$   
347 and a control  $\text{AcP10}^{\text{wt}}$  were used to infect TN368 cells at an MOI of 10, which were examined  
348 subsequently using confocal microscopy. The images were obtained from a number of different  
349 cells at each time-point and are representative; the heterogeneous nature of the TN368 cell line  
350 was taken into account during the analysis.

351

352 Figure 4 shows P10 mutant and control structures at 72- (Fig. 4, upper panels) and 96 hpi (Fig. 4,  
353 lower panels) when under control of the *polh* promoter. The P10 structures of  $\text{AcP10}^{\text{wt}}$  exhibited  
354 the same profile as the wild-type AcMNPV structures at 72- and 96 hpi (compare Figure 4, left  
355 hand panels with Figure 1); both cytoplasmic filaments and peri-nuclear tubules were present.

356 Similar to the wild-type AcMNPV infection (Figure 1), a few cytoplasmic filaments were  
357 detached at 72 hpi; however, by 96 hpi all filaments appeared detached and a distinctive P10  
358 tubular structure surrounding the nucleus in a ring-like form was visible at both 72- and 96 hpi.  
359 This structure remained intact at 96 hpi and disjointed from the cytoplasmic filaments.

360

361 The P10 mutant structures of AcP10<sup>S92A</sup> were similar to those of AcP10<sup>wt</sup> and developed at the  
362 same time (Figure 4). However, the P10 mutant structures of AcP10<sup>S93A</sup> and AcP10<sup>S9293A</sup>  
363 revealed conformational differences when compared to the control AcP10<sup>wt</sup> (Figure 4). The ring-  
364 like form of P10 perinuclear tubule is absent and is replaced by thin filaments surrounding the  
365 nucleus at 96hpi in these mutants. The mutant cytoplasmic filaments were disorganised, and  
366 displayed thinner and rigid conformation at 72- and 96 hpi indicating a structural aberration. In  
367 addition, these filaments displayed a delay in detachment from the cell nucleus compared to  
368 those from AcP10<sup>wt</sup> infection (Figure 4) or wild-type AcMNPV (Figure 1). These results suggest  
369 that a single mutation of the P10 residue, serine 93, affects the organisation of P10 filaments and  
370 consequently disrupts their detachment from the nucleus. It does not, however, completely  
371 abolish the detachment as some filaments were detached from the nucleus at both 72- and 96 hpi.  
372 The detachment was further analysed in relation to the microtubules. The co-localisation of P10  
373 mutant structures with microtubules was compared to that of the wildtype (Figure 4).

374

#### 375 **4. Mass spectrometric analysis of the C-terminus of P10 mutants**

376 MALDI-TOF mass spectrometry was employed to identify the site of phosphorylation in  
377 AcMNPV P10. This was done by analysing the phosphorylation associated mass shifts in the  
378 mutant and the wild-type P10. The consensus sequence for PKA includes the motif  $XXS(T)X$   
379 (R: Arginine, K: Lysine, X: any amino acid, S: Serine, T: Threonine) (25) and serine 93 of P10



380 fulfils this requirement (last 5 residues of P10 are KRSS\*K; \*serine 93). Therefore, serine 93  
381 mutant of P10 was selected for mass spectrometric analysis. Furthermore, P10 C-terminus has  
382 been shown to be efficiently phosphorylated by PKA (15).

383  
384 The MALDI-TOF analysis was performed following infection of *T. ni* cells with recombinant  
385 viruses AcP10<sup>S93A</sup> and AcP10<sup>wt</sup> at an MOI of 10. The MALDI-TOF spectrum was analysed for  
386 peaks corresponding to the C-terminal peptides containing serine 93 (unmodified) or alanine 93  
387 (mutant) residues from AcP10<sup>wt</sup> and AcP10<sup>S93A</sup>, respectively.

388  
389 Figure 5 shows the MALDI-TOF spectra containing the mass-to-charge ratio (m/z) peaks  
390 corresponding to the C-terminal peptide <sup>82</sup>LDSDARRGKRS(S/A)K<sup>94</sup>, a product of the  
391 endoproteinase GluC digestion of P10. In these spectra, the labelled m/z peaks correspond to the  
392 P10 C-terminal peptide <sup>82</sup>LDSDARRGKRSSK<sup>94</sup> ([M+H]<sup>+</sup> 1475.81, calculated mass  
393 1475.80) or <sup>82</sup>LDSDARRGKRSAK<sup>94</sup> ([M+H]<sup>+</sup> 1459.85, calculated mass 1459.81).  
394 Phosphorylation of the P10 C-terminal peptide from AcP10<sup>wt</sup> is evident by the presence of the  
395 peak [M+H]<sup>+</sup> 1555.75 corresponding to the peptide <sup>82</sup>LDSDARRGKRSSK<sup>94</sup> + 1P (PO<sub>3</sub><sup>2-</sup>),  
396 calculated mass 1555.77. However, in the spectra of the P10 mutant peptide from AcP10<sup>S93A</sup>, no  
397 peak is detected at 1539.81, the mass of phosphorylated peptide <sup>82</sup>LDSDARRGKRSAK<sup>94</sup> + 1P  
398 (PO<sub>3</sub><sup>2-</sup>).

399  
400 These data confirm, by exclusion, that the P10 residue serine 93, and not serine 92, is the  
401 substrate residue for a kinase. The presence of the phosphorylated P10 peptide from  
402 AcP10<sup>wt</sup> provides further evidence of phosphorylation in native P10.

403

404

## 405 **5. Circular Dichroism**

406 The Circular dichroism (CD) profile of a protein varies with the different secondary structure  
407 elements or folds. Circular dichroism was, therefore, used to analyse the secondary structure of  
408 wild-type P10 and its serine 93 mutant in order to determine whether phosphorylation may affect  
409 secondary structure characteristics.

410

411 Purified protein samples were prepared for CD spectroscopy using the recombinant viruses  
412 AcFBU-His-P10<sup>wt</sup> and AcFBU-His-P10<sup>S93A</sup> encoding His-tagged wild-type and mutant (serine  
413 93) P10 respectively (Figure 3). The CD profile of the wild-type P10 showed minima at 221 nm  
414 and at 208 nm; the serine 93 mutant, at 228.5 nm and at 205-215 nm (Figure 6). To determine the  
415 secondary structure of the serine 93 mutant and wild-type P10 from the CD spectra,  
416 deconvolution analysis of the spectra was performed using a linear combination of CD spectrum  
417 or LINCMB method. This method uses an algorithm based on a least-squares fit and a set of  
418 reference spectra (23). For the P10 CD spectra analysis, the set comprised of typical CD curves  
419 of  $\alpha$ -helix,  $\beta$ -pleated sheet (antiparallel),  $\beta$ -turns, disordered protein, and aromatic/disulphide (or  
420 non-peptide).

421

422 Deconvolution of the P10 wild-type spectrum showed that the protein comprised of  $\alpha$ -helix  
423 (47.86%) followed by  $\beta$ -turns (32.09%) while the remaining structure was random coil (20.05%).  
424 In comparison, the P10 serine 93 mutant revealed slightly reduced content of  $\alpha$ -helix (43.31%)  
425 and higher content of  $\beta$ -turns (37.79%). The percentage content of random coil in the two  
426 samples did not vary.

427

428

429 **Discussion**

430 The formation of P10 cytoskeletal-like structures during AcMNPV infection has been established  
431 in a number of previous studies (12–14). In this study, examination of P10 structures at 48-, 72-  
432 and 96 hpi using confocal microscopy revealed that they undergo a transition during this period  
433 of the AcMNPV infection cycle. The P10 tubular structure, which surrounded the host nucleus,  
434 was present from 48 hpi and developed into a discrete ring-like form disjointed from the P10  
435 cytoplasmic filaments by 96 hpi. In contrast, the P10 cytoplasmic filaments became detached and  
436 disintegrated by 96 hpi. Previously (14), these structures were described at 48 hpi. To better  
437 understand the significance of P10 structures during infection, we analysed how these structures  
438 transform until a very late time point such as 96 hpi when cells undergo lysis. These results are  
439 also consistent with the findings from the pulse-labelling experiments (24) that reported high  
440 level synthesis of P10 from 33 to 99 hpi. The fact that P10 continues to form structures in the  
441 host cell following the viral replication cycle is one of the key findings of this study. This  
442 phenomenon is indeed indicative of the requirement of this protein at this post-replication stage.

443

444 Phosphorylation of P10 has been postulated in a number of previous studies (12, 14, 15);  
445 however, there was no evidence to suggest that the phenomenon occurred in the wild-type virus  
446 infection. Herein, we report phosphorylation of P10 in wild-type AcMNPV infection at 7hpi  
447 using mass spectrometric analysis of P10 (Figure 2); however, this was a small proportion in  
448 comparison to the non-phosphorylated peptide. But considering technical limitations, the  
449 amount of phosphorylated peptide observed in this assay may not be truly reflective of the total  
450 amount of phosphorylated P10 present during infection. MALDI-TOF analysis of P10 mutants  
451 found that the C-terminal residue, serine 93, is the site of phosphorylation (Figure 5). This

452 phosphorylation site is conserved in P10 sequences from six members of alphabaculoviruses and  
453 there are potential phosphorylation sites in the C-terminal basic domain of P10 whose  
454 distribution is highly conserved in alphabaculovirus P10 homologues (7). Baculoviruses are  
455 known to encode several kinases that include serine/threonine kinases PK-1 and PK-2, which are  
456 expressed very-late or late respectively (26, 27). Thus, it is likely that P10 is phosphorylated by  
457 PK-1 or -2 encoded by the virus.

458

459 Phosphorylated P10 was also found in the cells infected with the recombinant viruses AcP10<sup>wt</sup>.  
460 This suggested that the dynamics of P10 phosphorylation in the recombinant viruses were  
461 comparable to the wild-type infection and thus unaffected by the use of the polyhedrin promoter.  
462 Phosphorylation was inhibited in the mutant P10 from cells infected with the recombinant virus  
463 AcP10<sup>S93A</sup> in which the phosphorylation site, serine 93, was substituted with alanine.

464

465 P10 structures of AcP10<sup>S93A</sup> and AcP10<sup>S9293A</sup> revealed significant differences compared to the  
466 wild-type control virus AcP10<sup>wt</sup> (Figure 4) and wild-type virus (Figure 1). Mutation of the  
467 phosphorylation site serine 93 resulted in aberrant formation of the P10 peri-nuclear tubules; it  
468 also affected the conformation of the cytoplasmic filaments. Therefore, it is very likely that  
469 phosphorylation of the P10 C-terminus facilitates aggregation of P10 in order to form the much  
470 distinctive tubular structures in the final stages of the infection. The timing of P10  
471 phosphorylation (72hpi) observed in the mass spectrometry data also correlates with the  
472 formation of these structures. The serine 93 mutants also showed a delay in the detachment of  
473 filaments from the nucleus suggesting that the aggregated filaments facilitated this process.  
474 Indeed phosphorylation modulates the aggregation propensity of several proteins and peptides  
475 (28–30); these include tau, synuclein and peptide model systems. Aggregation of self-assembling

476 proteins is particularly regulated by phosphorylation (31) and this may also be true for P10,  
477 which also self-assembles (32).

478  
479 The changes observed in the P10 mutant structures are unlikely to be caused by the substitution  
480 of serine with alanine at position 93 as both alanine and serine have neutral p*H*. Additionally, the  
481 observation that the P10 structures of the serine 92 mutant are similar to wild-type P10 structures  
482 further confirms that a single substitution of serine with alanine, in close proximity of the  
483 penultimate residue, does not have any observable influence on protein conformation.

484  
485 This study analysed the secondary structure of wild-type and serine 93 mutant P10 using the CD  
486 spectroscopy. No previous work has been done to reveal the secondary structure of P10. A  
487 reduction in the  $\alpha$ -helical content of the P10 was observed upon mutation of serine 93. Although  
488 not analysed, the serine 92 mutant most likely retained the wildtype conformation as no  
489 differences were observed in the P10 structures with confocal microscopy. Moreover, results  
490 from the secondary structure prediction software PSIPRED showed no differences in the  
491 secondary structure of P10 upon substitution of serine 92 or serine 93 with alanine. Therefore, it  
492 is unlikely that the substitution of serine 92 or 93 with alanine produced a significant change in  
493 the secondary structure of P10 unless there is a post-translational modification of the protein.  
494 Thus, the change in secondary structure could be a result of the addition of a phosphate moiety to  
495 a protein that is known to affect the electrostatic forces in a protein determining its folding. The  
496 type and extent of change in the folding varies with the location of the phosphorylation and is not  
497 entirely predictable. It is likely that the phosphorylation of the P10 penultimate residue plays a  
498 role in the stabilisation of the entire protein.

499

500 Taken together, the results of this study support the hypothesis that the phosphorylation of P10 at  
501 the C-terminus regulates its structural organisation. This phenomenon could be involved in  
502 multiple roles of P10 during virus infection. The P10 peri-nuclear tubules surround the polyhedra  
503 inside the cell nucleus, which indicates that they may have a protective role in the terminal stages  
504 of infection. These tubules may also stabilise the host nucleus to allow complete maturation of  
505 polyhedra to take place. Without the tubules, the polyhedra may be susceptible to digestion by  
506 viral cathepsin that is activated upon cell death. (33). This could also explain the results from an  
507 early study by Gross *et al.* (10) in which the periphery of the polyhedra were affected upon  
508 deletion of the *p10* gene. The phosphorylation driven aggregation of P10 cytoplasmic filaments  
509 may also be involved in timely destruction of the host cell to release the viral enzymes. This is  
510 consistent with the study in which deletion of P10 delayed the release of chitinase by 24 hours  
511 (33).

512

513 Microtubule associated proteins (MAPs) such as tau have a basic C-terminus that interacts with  
514 the negatively charged residues in tubulin (34). Phosphorylation of the MAP tau allows it to  
515 dissociate from the MTs because of the negative charge introduced by phosphorylation (35).  
516 Furthermore, aggregation of tau is also facilitated by phosphorylation (36). The C-terminus of  
517 P10, which is also the site of phosphorylation, is basic in nature since it is rich in lysine and  
518 arginine residues. Similar to the tau protein, the interaction of P10 with MTs may be facilitated  
519 through these basic residues and phosphorylation of P10 may influence its affinity for MTs and  
520 self-aggregation preproperties. Although no differences were observed in the co-alignment of  
521 mutant filaments with MTs in comparison to the wild-type, the mutants showed rigid  
522 conformation and a delayed detachment from the nucleus (results not shown). These  
523 observations could be the result of the altered affinity of P10 structures for MTs upon the

524 inhibition of phosphorylation. Testing this model could explain one of the mechanisms through  
525 which baculoviruses are able to take control of the host cytoskeleton.

526

## 527 **Acknowledgements**

528 The authors are grateful to Professor John Runions (Oxford Brookes University) and Dr David  
529 Staunton (University of Oxford) for their technical expertise with confocal microscopy and  
530 circular dichroism, respectively. The latter work was performed at University of Oxford with a  
531 research grant from the Santander Group.

532

## 533 **References**

- 534 1. **Federici BA**. 1986. Ultrastructure of baculoviruses, p. 61–88. *In* Granados, RR, Federici,  
535 BA (eds.), *The Biology of Baculoviruses*. CRC Press, Boca Raton, Fla.
- 536 2. **Vaughn JL, Faulkner P**. 1963. Susceptibility of an insect tissue culture to infection by  
537 virus preparations of the nuclear polyhedrosis of the silkworm (*bombyx mori* l.). *Virology*  
538 **20**:484–489.
- 539 3. **Summers MD, Volkman LE**. 1976. Comparison of biophysical and morphological  
540 properties of occluded and extracellular nonoccluded baculovirus from *in vivo* and *in vitro*  
541 host systems. *J Virol* **17**:962–972.
- 542 4. **Bilimoria S**. 1986. Taxonomy and identification of baculoviruses, p. 37–59. *In* Granados,  
543 R, Federeci, B (eds.), *The biology of baculoviruses*. CRC Press, Boca Raton, Fla.
- 544 5. **Thiem SM, Miller LK**. 1990. Differential gene expression mediated by late, very late and  
545 hybrid baculovirus promoters. *Gene* **91**:87–94.
- 546 6. **Rohel DZ, Cochran MA, Faulkner P**. 1983. Characterization of two abundant mRNAs of  
547 *Autographa californica* nuclear polyhedrosis virus present late in infection. *Virology*  
548 **124**:357–365.
- 549 7. **Carpentier DCJ, King LA**. 2009. The long road to understanding the baculovirus P10  
550 protein. *Virol Sin* **24**:227–242.
- 551 8. **Vlak JM, Klinkenberg FA, Zaal KJ, Usmany M, Klinge-Roode EC, Geervliet JB,**  
552 **Roosien J, van Lent JW**. 1988. Functional studies on the p10 gene of *Autographa*  
553 *californica* nuclear polyhedrosis virus using a recombinant expressing a p10-beta-  
554 galactosidase fusion gene. *J Gen Virol* **69 ( Pt 4)**:765–776.

- 555 9. **Williams GV, Rohel DZ, Kuzio J, Faulkner P.** 1989. A cytopathological investigation of  
556 *Autographa californica* nuclear polyhedrosis virus p10 gene function using  
557 insertion/deletion mutants. *J Gen Virol* **70 ( Pt 1)**:187–202.
- 558 10. **Gross CH, Russell RL, Rohrmann GF.** 1994. *Orgyia pseudotsugata* baculovirus p10 and  
559 polyhedron envelope protein genes: analysis of their relative expression levels and role in  
560 polyhedron structure. *J Gen Virol* **75 ( Pt 5)**:1115–1123.
- 561 11. **Summers MD, Arnott HJ.** 1969. Ultrastructural studies on inclusion formation and virus  
562 occlusion in nuclear polyhedrosis and granulosis virus-infected cells of *Trichoplusia ni*  
563 (*Hübner*). *J Ultrastruct Res* **28**:462–480.
- 564 12. **Quant-Russell RL, Pearson MN, Rohrmann GF, Beaudreau GS.** 1987.  
565 Characterization of baculovirus p10 synthesis using monoclonal antibodies. *Virology*  
566 **160**:9–19.
- 567 13. **Patmanidi AL, Possee RD, King LA.** 2003. Formation of P10 tubular structures during  
568 AcMNPV infection depends on the integrity of host-cell microtubules. *Virology* **317**:308–  
569 320.
- 570 14. **Carpentier DCJ, Griffiths CM, King LA.** 2008. The baculovirus P10 protein of  
571 *Autographa californica* nucleopolyhedrovirus forms two distinct cytoskeletal-like  
572 structures and associates with polyhedral occlusion bodies during infection. *Virology*  
573 **371**:278–291.
- 574 15. **Cheley S, Kosik KS, Paskevich P, Bakalis S, Bayley H.** 1992. Phosphorylated  
575 baculovirus p10 is a heat-stable microtubule-associated protein associated with process  
576 formation in Sf9 cells. *J Cell Sci* **102 ( Pt 4)**:739–752.
- 577 16. **Luckow VA, Summers MD.** 1988. Trends in the Development of Baculovirus Expression  
578 Vectors. *Nat Biotechnol* **6**:47–55.
- 579 17. **Vaughn JL, Goodwin RH, Tompkins GJ, McCawley P.** 1977. The establishment of two  
580 cell lines from the insect *Spodoptera frugiperda* (Lepidoptera; Noctuidae). *In Vitro* **13**:213–  
581 217.
- 582 18. **Granados RR, Guoxun L, Derksen ACG, McKenna KA.** 1994. A new insect cell line  
583 from *Trichoplusia ni* (BTI-Tn-5B1-4) susceptible to *Trichoplusia ni* single enveloped  
584 nuclear polyhedrosis virus. *Journal of invertebrate pathology* **64**:260–266.
- 585 19. **Hink WF.** 1970. Established insect cell line from the cabbage looper, *Trichoplusia ni*.  
586 *Nature* **226**:466–467.
- 587 20. **Possee RD.** 1986. Cell-surface expression of influenza virus haemagglutinin in insect cells  
588 using a baculovirus vector. *Virus Res* **5**:43–59.
- 589 21. **Vandeyar MA, Weiner MP, Hutton CJ, Batt CA.** 1988. A simple and rapid method for  
590 the selection of oligodeoxynucleotide-directed mutants. *Gene* **65**:129–133.



- 591 22. **King LA, Possee RD.** 1992. The baculovirus expression system : a laboratory guide.  
592 Chapman & Hall, London; New York, N.Y.
- 593 23. **Perczel A, Park K, Fasman GD.** 1992. Analysis of the circular dichroism spectrum of  
594 proteins using the convex constraint algorithm: a practical guide. *Anal Biochem* **203**:83–  
595 93.
- 596 24. **Smith GE, Vlak JM, Summers MD.** 1983. Physical Analysis of *Autographa californica*  
597 Nuclear Polyhedrosis Virus Transcripts for Polyhedrin and 10,000-Molecular-Weight  
598 Protein. *J Virol* **45**:215–225.
- 599 25. **Hennrich ML, Marino F, Groenewold V, Kops GJPL, Mohammed S, Heck AJR.**  
600 2013. Universal quantitative kinase assay based on diagonal SCX chromatography and  
601 stable isotope dimethyl labeling provides high-definition kinase consensus motifs for PKA  
602 and human Mps1. *J Proteome Res* **12**:2214–2224.
- 603 26. **Reilly LM, Guarino LA.** 1994. The pk-1 gene of *Autographa californica*  
604 multinucleocapsid nuclear polyhedrosis virus encodes a protein kinase. *J Gen Virol* **75** ( Pt  
605 **11**):2999–3006.
- 606 27. **Li Y, Miller LK.** 1995. Expression and functional analysis of a baculovirus gene encoding  
607 a truncated protein kinase homolog. *Virology* **206**:314–323.
- 608 28. **Schneider A, Biernat J, von Bergen M, Mandelkow E, Mandelkow EM.** 1999.  
609 Phosphorylation that detaches tau protein from microtubules (Ser262, Ser214) also protects  
610 it against aggregation into Alzheimer paired helical filaments. *Biochemistry* **38**:3549–3558.
- 611 29. **Paleologou KE, Schmid AW, Rospigliosi CC, Kim H-Y, Lamberto GR, Fredenburg**  
612 **RA, Lansbury PT, Fernandez CO, Eliezer D, Zweckstetter M, Lashuel HA.** 2008.  
613 Phosphorylation at Ser-129 but not the phosphomimics S129E/D inhibits the fibrillation of  
614 alpha-synuclein. *J Biol Chem* **283**:16895–16905.
- 615 30. **Kühnle H, Börner HG.** 2009. Biotransformation on polymer-peptide conjugates: a  
616 versatile tool to trigger microstructure formation. *Angew Chem Int Ed Engl* **48**:6431–6434.
- 617 31. **Valette NM, Radford SE, Harris SA, Warriner SL.** 2012. Phosphorylation as a tool to  
618 modulate aggregation propensity and to predict fibril architecture. *Chembiochem* **13**:271–  
619 281.
- 620 32. **Alaoui-Ismaili MH, Richardson CD.** 1998. Insect virus proteins (FALPE and p10) self-  
621 associate to form filaments in infected cells. *J Virol* **72**:2213–2223.
- 622 33. **Thomas CJ, Brown HL, Hawes CR, Lee BY, Min MK, King LA, Possee RD.** 1998.  
623 Localization of a baculovirus-induced chitinase in the insect cell endoplasmic reticulum. *J*  
624 *Virol* **72**:10207–10212.
- 625 34. **Morris M, Maeda S, Vossel K, Mucke L.** 2011. The many faces of tau. *Neuron* **70**:410–  
626 426.

- 627 35. **Bramblett GT, Goedert M, Jakes R, Merrick SE, Trojanowski JQ, Lee VM.** 1993.  
628 Abnormal tau phosphorylation at Ser396 in Alzheimer's disease recapitulates development  
629 and contributes to reduced microtubule binding. *Neuron* **10**:1089–1099.
- 630 36. **Alonso A, Zaidi T, Novak M, Grundke-Iqbal I, Iqbal K.** 2001. Hyperphosphorylation  
631 induces self-assembly of tau into tangles of paired helical filaments/straight filaments. *Proc*  
632 *Natl Acad Sci U S A* **98**:6923–6928.

633

634

635

### 636 **Figure Legends**

637 **Figure 1. Temporal changes in the P10 structures during AcMNPV infection of TN368**  
638 **cells.** (A) The amino acid sequence of AcMNPV P10 reveals three distinct regions, a coiled-coil  
639 domain at the N-terminus (blue residues), a proline-rich region in the variable region (green  
640 residues) and a positively charged basic region at the C-terminus (red residues; R: Arginine, K:  
641 Lysine). Amino acid residues of the heptad repeat in the coiled-coil region are denoted as  
642 *abcdefg*, in which *a* and *d* are hydrophobic whereas *e* and *g* are charged residues. (B) Wildtype-  
643 infected TN368 cells were analysed at 48-, 72- and 96 hpi using confocal laser scanning  
644 microscopy. Cells were stained with anti-P10- and Alexa Fluor 488 antibody to visualise P10  
645 (green) and with anti- $\alpha$ -Tubulin- and Alexa Fluor 568 antibody to visualise MTs (red). P10 and  
646  $\alpha$ -Tubulin channels were merged to show co-alignment. Position of OB-filled nucleus is shown  
647 in the bright field images. At 48- and 72 hpi, P10 filaments were co-aligned with MTs and  
648 spanned the host cytoplasm; bundling of these filaments was evident at 72 hpi. P10 also formed  
649 peri-nuclear tubular structures that were present from 48 hpi and most developed at 96 hpi. The  
650 P10 cytoplasmic filaments appeared detached from the peri-nuclear tubule and partially  
651 disintegrated at 96 hpi. Scale bars, 30  $\mu$ m.

652

653 **Figure 2. MALDI-TOF mass spectrometric analysis of the P10 C-terminus.** The AcMNPV  
654 P10 protein was harvested at 72 hpi and digested with endoproteinase GluC to cleave peptide  
655 bonds C-terminal to glutamic acid residues. The peptide products were analysed by MALDI-  
656 TOF MS (Ultraflex™, Bruker Daltonics) in linear mode. Image shows a portion of the spectrum  
657 containing the peptides of interest from P10 C-terminus. The x-axis represents mass divided by  
658 charge (m/z) and the y-axis represents absolute intensity. Peaks with m/z values of 1475.81 and  
659 1555.75 corresponded to the non- and mono-phosphorylated states of the P10 C-terminus  
660 peptide <sup>82</sup>LDSDARRGKRSSK<sup>94</sup>.

661  
662 **Figure 3. Construction of recombinant viruses.** (A) Wild-type or mutant *p10* flanked by *XbaI*  
663 and *XmaI* restriction sites was inserted downstream of the polyhedrin promoter in the transfer  
664 vector pBacPAK8. Recombinant baculoviruses were made by allowing homologous  
665 recombination of the transfer vector and *flashBACULTRA*. Four viruses were constructed; in  
666 single mutants, AcP10<sup>S92A</sup> and AcP10<sup>S93A</sup>, serine 92 and 93 were mutated to alanine respectively.  
667 In the double mutant, AcP10<sup>S9293A</sup>, both serine 92 and 93 were mutated to alanine.  
668 AcP10<sup>wt</sup> contained the wild-type *p10*. (B) pAcUW2B was used to construct the His-tagged wild-  
669 type and mutant *p10* encoding viruses. This vector included a complete *polh* gene. The P10  
670 fragment was inserted downstream of the P10 promoter in pAcUW2B using the *PstI* and *SpeI*  
671 restriction sites. Six histidine residues followed by the TEV cleavage site residues were added at  
672 the N-terminus. Two recombinant viruses were constructed by co-transfecting pAcUW2B  
673 modified vectors with *flashBACULTRA*: Ac-His-P10<sup>wt</sup>, containing wild-type *p10* gene and  
674 mutant Ac-His-P10<sup>S93A</sup>. Displayed genes are not to scale.

675

676 **Figure 4. Analysis of wild-type and mutant P10 structures.** TN368 cells were infected with  
677 AcP10<sup>wt</sup>, AcP10<sup>S92A</sup>, AcP10<sup>S93A</sup> or AcP10<sup>S9293A</sup> and then fixed at 72- and 96 hpi. P10 structures  
678 were visualised by anti-P10- and Alexa Fluor 488 antibody; microtubules(red) were visualised by  
679 anti- $\alpha$ Tubulin- and Alexa Fluor 568 antibody. P10 and  $\alpha$ -Tubulin channels were merged to show  
680 co-alignment. At 72 hpi, cells infected with AcP10<sup>wt</sup> or AcP10<sup>S92A</sup> showed both P10 peri-nuclear  
681 tubules (NT) and cytoplasmic filaments (CF). By 96 hpi, the peri-nuclear tubules had matured  
682 and most cytoplasmic filaments were detached from the central tubule. Cells infected with  
683 AcP10<sup>S93A</sup> or AcP10<sup>S9293A</sup> lacked peri-nuclear tubules and displayed rigid and angular  
684 cytoplasmic filaments that were not fully detached from the nucleus. Images are representative.  
685 Scale bars, 30  $\mu$ m.

686

687 **Figure 5. MALDI-TOF mass spectrometric analysis of the P10 peptides from AcP10<sup>wt</sup> and**  
688 **AcP10<sup>S93A</sup>.** In-gel digestion of P10 protein (separated by SDS-PAGE) from AcP10<sup>wt</sup> and  
689 AcP10<sup>S93A</sup> was carried out with endoproteinase GluC; this cleaved peptide bonds C-terminal to  
690 glutamic acid residues in ammonium carbonate buffer. The peptide fragments were analysed by  
691 MALDI-TOF MS (Ultraflex<sup>TM</sup>, Bruker Daltonics) in linear mode. Image shows a portion of the  
692 spectrum containing the P10 C-terminal peptides of interest. The x-axis represents mass-to-  
693 charge ratio (m/z) and the y-axis represents absolute intensity as measured by the detector. The  
694 top panel shows the MALDI-TOF spectrum of the P10 C-terminal peptide from AcP10<sup>wt</sup>, in  
695 which wild-type P10 expression was driven by the polyhedrin gene promoter. The MALDI-TOF  
696 spectrum shows peaks with m/z values of 1475.81 and 1555.75 that corresponded to the non- and  
697 mono-phosphorylated states of the P10 peptide <sup>82</sup>LDSDARRGKRSSK<sup>94</sup>. The bottom panel

698 shows the MALDI-TOF spectrum of the P10 peptide from AcP10<sup>S93A</sup>. In this recombinant virus,  
699 the P10 residue serine 93 was mutated to alanine and the mutant expression was driven by the  
700 *polh* promoter. The MALDI-TOF spectrum shows a signal at  $[M+H]^+$  1459.85 corresponding to  
701 the peptide <sup>82</sup>LDSDARRGKRS<sup>94</sup>AK, however, no phosphorylated form of this peptide was  
702 observed (no signal at m/z 1539).

703

704 **Figure 6. Secondary structure of wildtype P10 and its serine 93 mutant.** Spectra were  
705 averaged from 4 to 16 scans in the wavelength range 260–190 nm. CD was measured in  
706 ellipticity units, millidegrees (mdeg). The CD spectra of the serine 93 mutant and wildtype P10  
707 revealed differences in the minima. Table shows the percentage of different secondary structures  
708 in the two proteins following LINCOMB analysis of spectra.

709

710

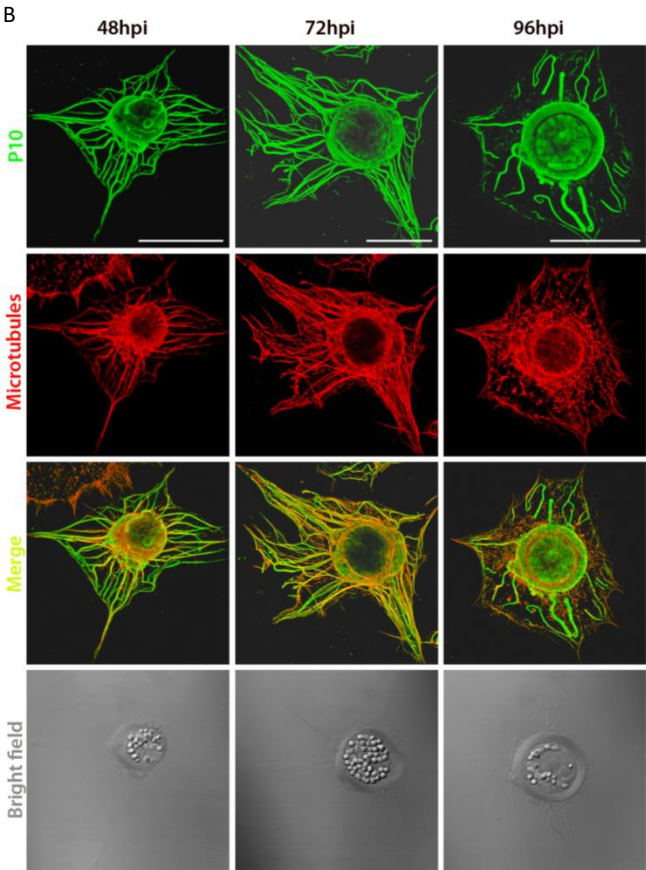


**Figure 1. Temporal changes in the P10 structures during AcMNPV infection of TN368 cells.** (A) The amino acid sequence of AcMNPV P10 reveals three distinct regions, a coiled-coil domain at the N-terminus (blue residues), a proline-rich region in the variable region (green residues) and a positively charged basic region at the C-terminus (red residues; R: Arginine, K: Lysine). Amino acid residues of the heptad repeat in the coiled-coil region are denoted as *abcdefg*, in which *a* and *d* are hydrophobic whereas *e* and *g* are charged residues. (B) Wildtype-infected TN368 cells were analysed at 48-, 72- and 96 hpi using confocal laser scanning microscopy. Cells were stained with anti-P10- and Alexa Fluor 488 antibody to visualise P10 (green) and with anti- $\alpha$ -Tubulin- and Alexa Fluor 568 antibody to visualise MTs (red). P10 and  $\alpha$ -Tubulin channels were merged to show co-alignment. Position of OB-filled nucleus is shown in the bright field images. At 48- and 72 hpi, P10 filaments were co-aligned with MTs and spanned the host cytoplasm; bundling of these filaments was evident at 72 hpi. P10 also formed peri-nuclear tubular structures that were present from 48 hpi and most developed at 96 hpi. The P10 cytoplasmic filaments appeared detached from the peri-nuclear tubule and partially disintegrated at 96 hpi. Scale bars, 30  $\mu$ m.

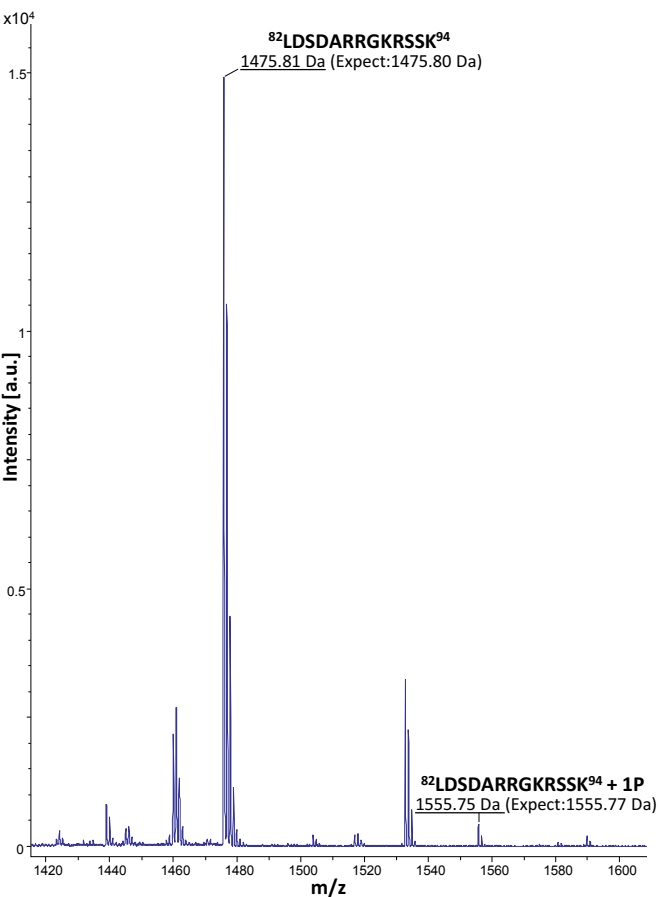


**Figure 2. MALDI-TOF mass spectrometric analysis of the P10 C-terminus.** The AcMNPV P10 protein was harvested at 72 hpi and digested with endoproteinase GluC to cleave peptide bonds C-terminal to glutamic acid residues. The peptide products were analysed by MALDI-TOF MS (UltraflexTM, Bruker Daltonics) in linear mode. Image shows a portion of the spectrum containing the peptides of interest from P10 C-terminus. The x-axis represents mass divided by charge (m/z) and the y-axis represents absolute intensity. Peaks with m/z values of 1475.81 and 1555.75 corresponded to the non- and mono-phosphorylated states of the P10 C-terminus peptide <sup>82</sup>LDS DARRGKRSSK<sup>94</sup>.

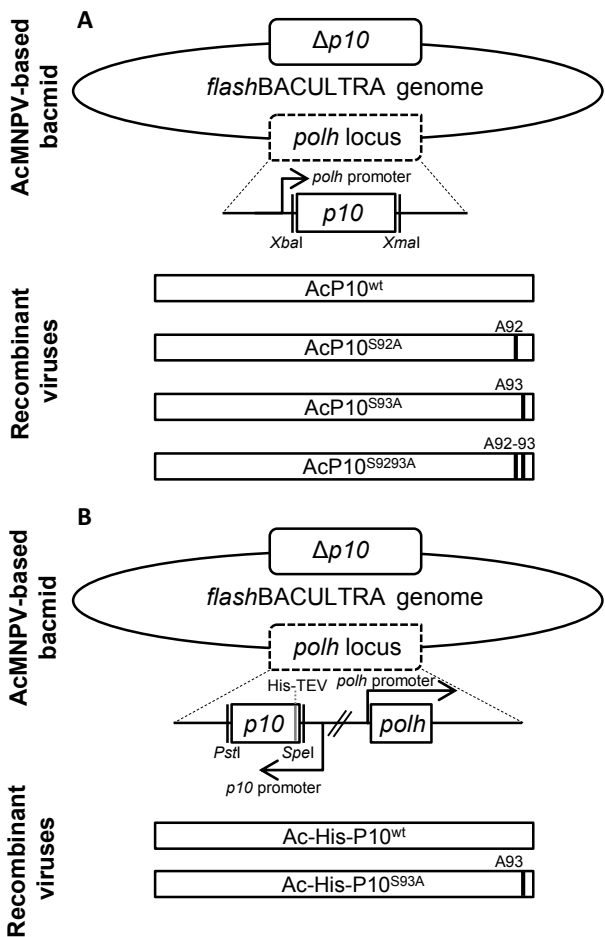


**Figure 3. Construction of recombinant viruses.** (A) Wild-type or mutant *p10* flanked by *Xba*I and *Xma*I restriction sites was inserted downstream of the polyhedrin promoter in the transfer vector pBacPAK8. Recombinant baculoviruses were made by allowing homologous recombination of the transfer vector and *flashBACULTRA*. Four viruses were constructed; in single mutants, AcP10<sup>S92A</sup> and AcP10<sup>S93A</sup>, serine 92 and 93 were mutated to alanine respectively. In the double mutant, AcP10<sup>S9293A</sup>, both serine 92 and 93 were mutated to alanine. AcP10<sup>wt</sup> contained the wild-type *p10*. (B) pAcUW2B was used to construct the His-tagged wild-type and mutant *p10* encoding viruses. This vector included a complete *polh* gene. The P10 fragment was inserted downstream of the P10 promoter in pAcUW2B using the *Pst*I and *Spe*I restriction sites. Six histidine residues followed by the TEV cleavage site residues were added at the N-terminus. Two recombinant viruses were constructed by co-transfecting pAcUW2B modified vectors with *flashBACULTRA*: Ac-His-P10<sup>wt</sup>, containing wild-type *p10* gene and mutant Ac-His-P10<sup>S93A</sup>. Displayed genes are not to scale.



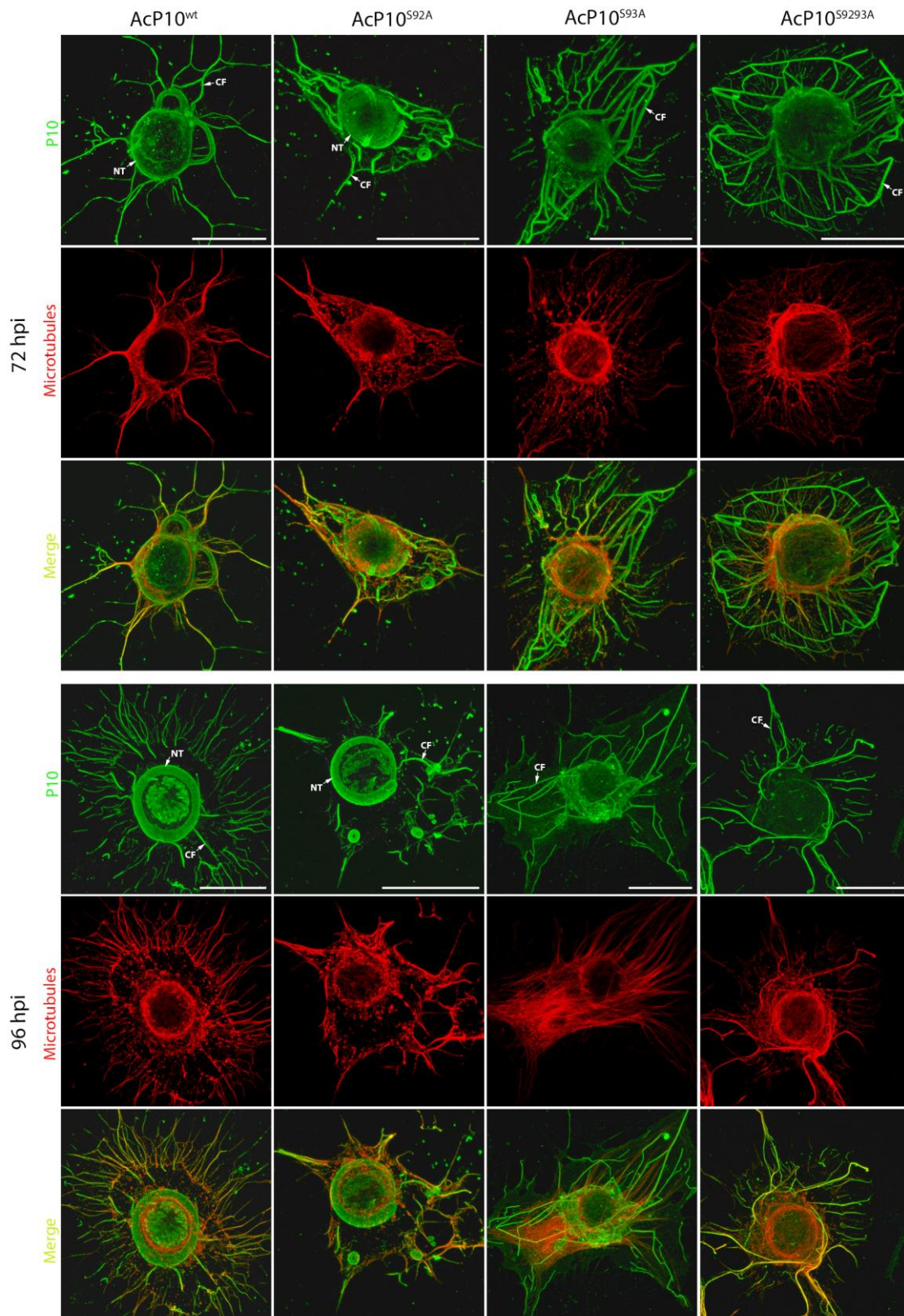


**Figure 4. Analysis of wild-type and mutant P10 structures.** TN368 cells were infected with AcP10<sup>wt</sup>, AcP10<sup>S92A</sup>, AcP10<sup>S93A</sup> or AcP10<sup>S9293A</sup> and then fixed at 72- and 96 hpi. P10 structures were visualised by anti-P10- and Alexa Fluor 488 antibody; microtubules (red) were visualised by anti- $\alpha$ Tubulin- and Alexa Fluor 568 antibody. P10 and  $\alpha$ -Tubulin channels were merged to show co-alignment. At 72 hpi, cells infected with AcP10<sup>wt</sup> or AcP10<sup>S92A</sup> showed both P10 peri-nuclear tubules (NT) and cytoplasmic filaments (CF). By 96 hpi, the peri-nuclear tubules had matured and most cytoplasmic filaments were detached from the central tubule. Cells infected with AcP10<sup>S93A</sup> or AcP10<sup>S9293A</sup> lacked peri-nuclear tubules and displayed rigid and angular cytoplasmic filaments that were not fully detached from the nucleus. Images are representative. Scale bars, 30  $\mu$ m.

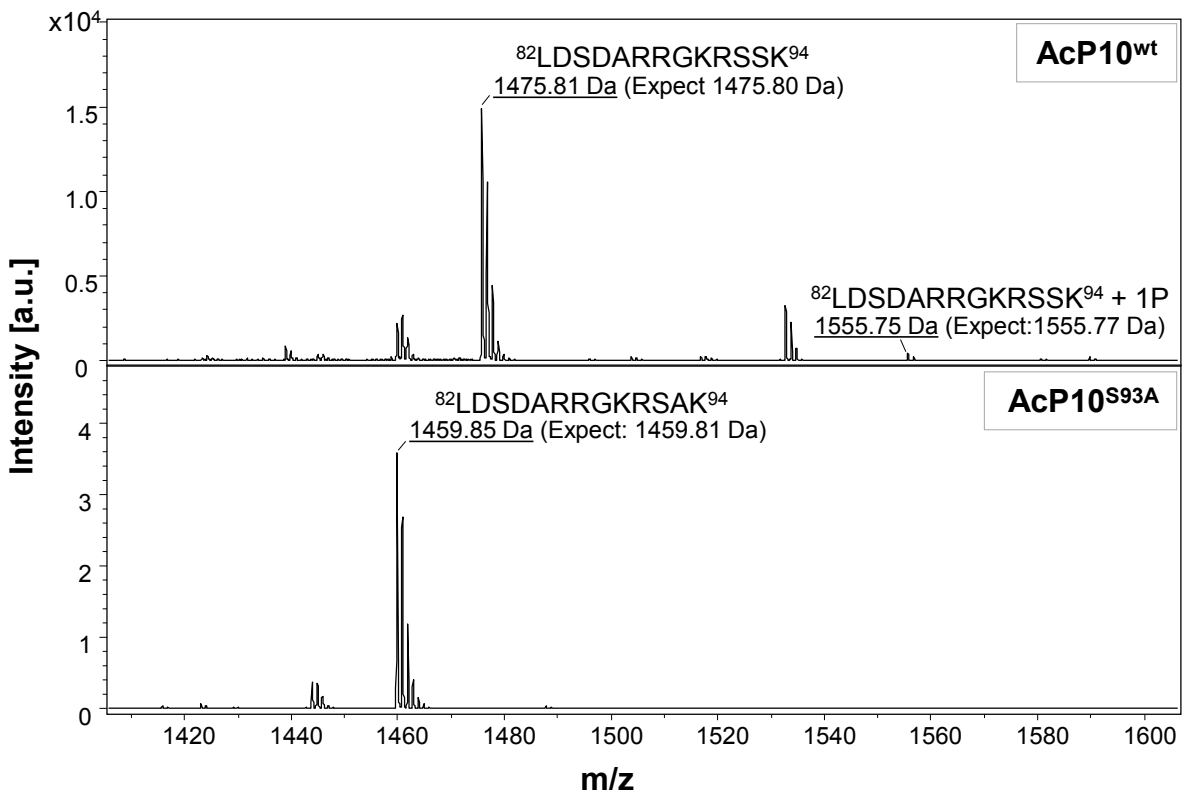
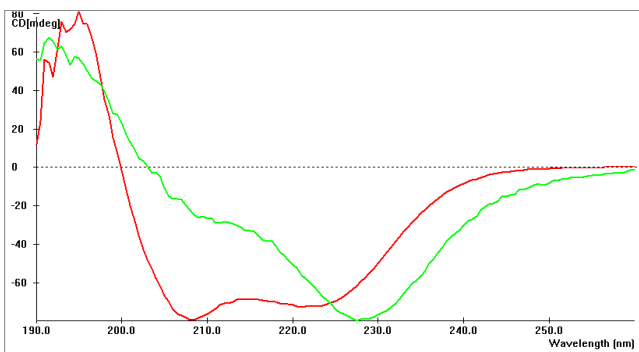


**Figure 5. MALDI-TOF mass spectrometric analysis of the P10 peptides from AcP10<sup>wt</sup> and AcP10<sup>S93A</sup>.** In-gel digestion of P10 protein (separated by SDS-PAGE) from AcP10<sup>wt</sup> and AcP10<sup>S93A</sup> was carried out with endoproteinase GluC; this cleaved peptide bonds C-terminal to glutamic acid residues in ammonium carbonate buffer. The peptide fragments were analysed by MALDI-TOF MS (Ultraflex™, Bruker Daltonics) in linear mode. Image shows a portion of the spectrum containing the P10 C-terminal peptides of interest. The x-axis represents mass-to-charge ratio (m/z) and the y-axis represents absolute intensity as measured by the detector. The top panel shows the MALDI-TOF spectrum of the P10 C-terminal peptide from AcP10<sup>wt</sup>, in which wild-type P10 expression was driven by the polyhedrin gene promoter. The MALDI-TOF spectrum shows peaks with m/z values of 1475.81 and 1555.75 that corresponded to the non- and mono-phosphorylated states of the P10 peptide <sup>82</sup>LDSDARRGKRSSK<sup>94</sup>. The bottom panel shows the MALDI-TOF spectrum of the P10 peptide from AcP10<sup>S93A</sup>. In this recombinant virus, the P10 residue serine 93 was mutated to alanine and the mutant expression was driven by the *polh* promoter. The MALDI-TOF spectrum shows a signal at [M+H]<sup>+</sup> 1459.85 corresponding to the peptide <sup>82</sup>LDSDARRGKRSAK<sup>94</sup>, however, no phosphorylated form of this peptide was observed (no signal at m/z 1539).



Protein	$\alpha$ -helix (%)	$\beta$ -Turn (%)	Random coil (%)	Error (SD)
P10 wild-type	47.86	32.09	20.05	0.950
P10 mutant (S93A)	43.31	37.79	18.90	0.855

**Figure 6. Secondary structure of wildtype P10 and its serine 93 mutant.** Spectra were averaged from 4 to 16 scans in the wavelength range 260–190 nm. CD was measured in ellipticity units, millidegrees (mdeg). The CD spectra of the serine 93 mutant and wildtype P10 revealed differences in the minima. Table shows the percentage of different secondary structures in the two proteins following LINCOMB analysis of spectra.